Nanoelectronics and Its New Materials – A NEW ERA OF NANOSCIENCE

Nanoelectronics and Its New Materials –

A NEW ERA OF NANOSCIENCE

ZEISS
Seeing beyond

WILEY

Discover the recent advances in electronics research and fundamental nanoscience.

Nanotechnology has become the driving force behind breakthroughs in engineering, materials science, physics, chemistry, and biological sciences. In this compendium, we delve into a wide range of novel applications that highlight recent advances in electronics research and fundamental nanoscience. From surface analysis and defect detection to tailored optical functionality and transparent nanowire electrodes, this eBook covers key topics that will revolutionize the future of electronics.

To get your hands on this valuable resource and unleash the power of nanotechnology, simply download the eBook now. Stay ahead of the curve and embrace the future of electronics with nanoscience as your guide.

ZEISS
Seeing beyond

WILEY

Mechanistic Observation of Interactions between Macrophages and Inorganic Particles with Different Densities

Chengchen Zhang, Jianbo Tang, Wanjie Xie, Francois-Marie Allioux, Zhenbang Cao, Joanna M. Biazik, Mohammad Tajik, Fei Deng, Yi Li, Roozbeh Abbasi, Mahroo Baharfar, Maedehsadat Mousavi, Dorna Esrafilzadeh, and Kourosh Kalantar-Zadeh*

Many different types of inorganic materials are processed into nano/microparticles for medical utilization. The impact of selected key characteristics of these particles, including size, shape, and surface chemistries, on biological systems, is frequently studied in clinical contexts. However, one of the most important basic characteristics of these particles, their density, is yet to be investigated. When the particles are designed for drug delivery, highly mobile macrophages are the major participants in cellular levels that process them in vivo. As such, it is essential to understand the impact of particles' densities on the mobility of macrophages. Here, inorganic particles with different densities are applied, and their interactions with macrophages studied. A set of these particles are incubated with the macrophages and the outcomes are explored by optical microscopy. This microscopic view provides the understanding of the mechanistic interactions between particles of different densities and macrophages to conclude that the particles' density can affect the migratory behaviors of macrophages: the higher the density of particles engulfed inside the macrophages, the less mobile the macrophages become. This work is a strong reminder that the density of particles cannot be neglected when they are designed to be utilized in biological applications.

1. Introduction

To date, numerous inorganic materials have been processed into nano/microparticles for exploring their potential for medical utilization such as drug delivery,[1–3] cancer therapy,[4,5] and biomedical sensing.[6,7] For translating these particles from laboratory research into clinical contexts, investigating different key physical characteristics, such as size, shape, and hardness,[8,9] and also surface chemistry, are essential as they critically affect the behaviors of biological systems.[10,11] It has been reported that nano/microparticles with different sizes could show various penetration depths in tumors.[12] Researchers have examined the impact of particle shapes to observe that some morphologies have longer blood circulation time and higher tumor uptake than others.[13] Besides, various surface

C. Zhang, J. Tang, W. Xie, F.-M. Allioux, Z. Cao, R. Abbasi, M. Baharfar, M. Mousavi, K. Kalantar-Zadeh
School of Chemical Engineering
University of New South Wales (UNSW)
Sydney, NSW 2052, Australia
E-mail: k.kalantar-zadeh@unsw.edu.au

W. Xie
Evolution and Optics of Nanostructures Group
Department of Biology
University of Ghent
K. L. Ledeganckstraat 35, Ghent 9000, Belgium

J. M. Biazik
Electron Microscope Unit
Mark Wainwright Analytical Centre
University of New South Wales (UNSW)
Sydney, NSW 2052, Australia

M. Tajik
School of Chemistry
University of New South Wales (UNSW)
Sydney, NSW 2052, Australia

F. Deng, Y. Li
ARC Centre of Excellence for Nanoscale BioPhotonics
Graduate School of Biomedical Engineering
University of New South Wales (UNSW)
Sydney, NSW 2052, Australia

D. Esrafilzadeh
Graduate School of Biomedical Engineering
University of New South Wales (UNSW)
Sydney, NSW 2052, Australia

K. Kalantar-Zadeh
School of Chemical and Biomolecular Engineering
The University of Sydney
Sydney, NSW 2006, Australia

**ADVANCED
SCIENCE NEWS**

www.advancedsciencenews.com

NANO · MICRO

small

www.small-journal.com

chemistries have been devised to explore their effects on the behaviors of nano/microparticles.[14,15] Although our understanding of the interactions between nano/microparticles and biological systems has critically advanced based on such investigations, one of the most important characteristics of nano/microparticles, density, is yet to be studied.

So far in biosystems, there have been very limited studies on the effect of particle densities on cells' behaviors, with the reported works mostly focused on the migration properties of nano/microparticles toward the vascular walls, an observation that is called margination. For example, researchers have shown that the density of particles affects their margination in blood flows,[16–18] and can influence the permeability of endothelial cells.[19] These works indicate that particle density is an important parameter for determining the efficacy of drug delivery. In fact, the margination affects the particles' targeting ability in blood circulation and thereafter influences their tissue accumulations.[20,21]

In physiology, the margination of white blood cells is critical for achieving their functions before migrating into tissues.[22] Macrophages are one of the white blood cell types, which are defenders against pathogens and scavengers by engulfing unhealthy cells and cell debris.[23] During inflammation, they can migrate from blood to tissues in response to antigens and then release pro-inflammatory mediators to stimulate the immune system.[24,25] Furthermore, as a family member of professional phagocytes, they move around to initiate the clearance of foreign nano/micro materials.[26,27] Therefore, the migration properties of macrophages play crucial roles during inflammatory responses[28] and phagocytosis.[29]

Different types of nano/microparticles have been used for drug delivery and macrophages have been reported to be the dominant cell type that interacts with those particles.[26,30,31] However, the investigation of the influence of particle densities on macrophages, especially on the migration properties has remained underexplored. Considering this important knowledge gap, we hypothesize that particle density may influence the migration of macrophages and hence influence their mechanistic behavior.

Driven by this hypothesis, we implemented inorganic nano/microparticles with different densities and studied their interactions with macrophages. A set of concentrations of these particles were delivered into RAW 264.7 macrophages; first, to assess their cytotoxicity. Guided by the safe doses, a group of particles with different concentrations was incubated with the macrophages and observed by high-resolution light microscopy. Under light microscopic imaging, the cellular endocytosis of particles into macrophages, and the migratory behaviors of macrophages were recorded. The cell migration velocities and trajectories were extracted from those recordings for analysis. The surface chemistries of the particles were assessed by measuring their zeta potentials and protein absorption to eliminate the possible interfering factors from the particle surfaces.

2. Results and Discussion

2.1. Preparation and Characterization of Particles

To study the effects of particle density on the behaviors of macrophages, we designed the scenarios of treating cells with different particles of various densities as shown in the

schematic in **Figure 1**a. The particles were sterilized by ethanol (EtOH) and then transferred into cell culture medium, Dulbecco's modified eagle's medium (DMEM), shortly before adding into macrophages. The migratory behaviors of the cells are observed and analyzed by optical microscopy.

The densities for the six types of nano/microparticles used in this work are provided in **Table 1**. The silica and gold (Au) particles, two of the most studied nano/microparticles among nanomaterials, were purchased to provide the densities at 1.98 and 19.32 g cm^{-3}. Another four types of metals (gallium (Ga), indium (In), bismuth (Bi), and tin(Sn)), which can be easily melted into a liquid and broken into nano/micro spheres by mechanical agitation, were chosen to provide densities from 5.91 to 9.75 g cm^{-3}. Those particles were synthesized by a probe sonication technique as illustrated in Figure S1, Supporting Information, and the detailed process is provided in the Experimental Section (preparation of liquid metal particles).

The scanning electron microscopy (SEM) images (Figure 1b) show all those particles have spherical morphologies and the analysis of the dimensions based on the SEM images show the size and distribution of those particles are as follows: 702 ± 40 nm (silica), 338 ± 95 nm (Ga), 949 ± 235 nm (Sn), 430 ± 179 nm (In), 727 ± 232 nm (Bi), and 376 ± 28 nm (Au). All the particles were observed to be engulfed equally successfully by the macrophages under transmission electron microscopy (TEM) shown in Figure S2, Supporting Information, and they are suggested to be internalized through phagocytosis (occurs predominantly in professional phagocytes) and macropinocytosis (for particle size range: 0.2–5 μm).[32,33] The hydrodynamic sizes of particles in the cell culture medium are measured and presented in Figure S3, Supporting Information, the particles' sizes are equal to or only slightly larger than the ones extracted from the SEM images, especially with the increased incubation time from 1 to 24 h. These results indicate that proteins and organic molecules from the cell culture medium may adhere to their surfaces of particles. To assess the surface properties of the six types of particles in the cell culture medium, the zeta potentials of the suspension of each particle type in DMEM were first measured. As shown in Figure 1d, the zeta potentials vary from −30 to −10 mV in the DMEM alone, while all zeta potentials increase and reach neutrality when incubated in DMEM supplemented with 10% fetal bovine serum (FBS). Additionally, after the incubation with DMEM, supplemented with 10% FBS, the zeta potentials for the particle suspensions were measured again after washing away the free FBS too, and in this case, no significant difference in the zeta potentials was observed. These results indicate that the measured changes of the zeta potentials for the particle suspensions, after the incubation with DMEM, supplemented with 10% FBS, are likely from the particles, and not from the free proteins in the supplemented FBS. The observation can be explained by the non-specific absorption of a protein layer, which is called "protein corona," on the surfaces of all the particles in the biological fluids.[32]

The liquid chromatography-mass spectrometry (LC-MS)/MS analysis presented in Figure 1e shows the protein layers for all the particles are dominantly composed of bovine serum albumin (ALBU-BOVIN, BSA) from the DMEM added with 10% FBS. Additionally, the compositions of the top ten proteins (BSA, hemoglobin fetal subunit beta (HBBF_BOVIN), hemoglobin
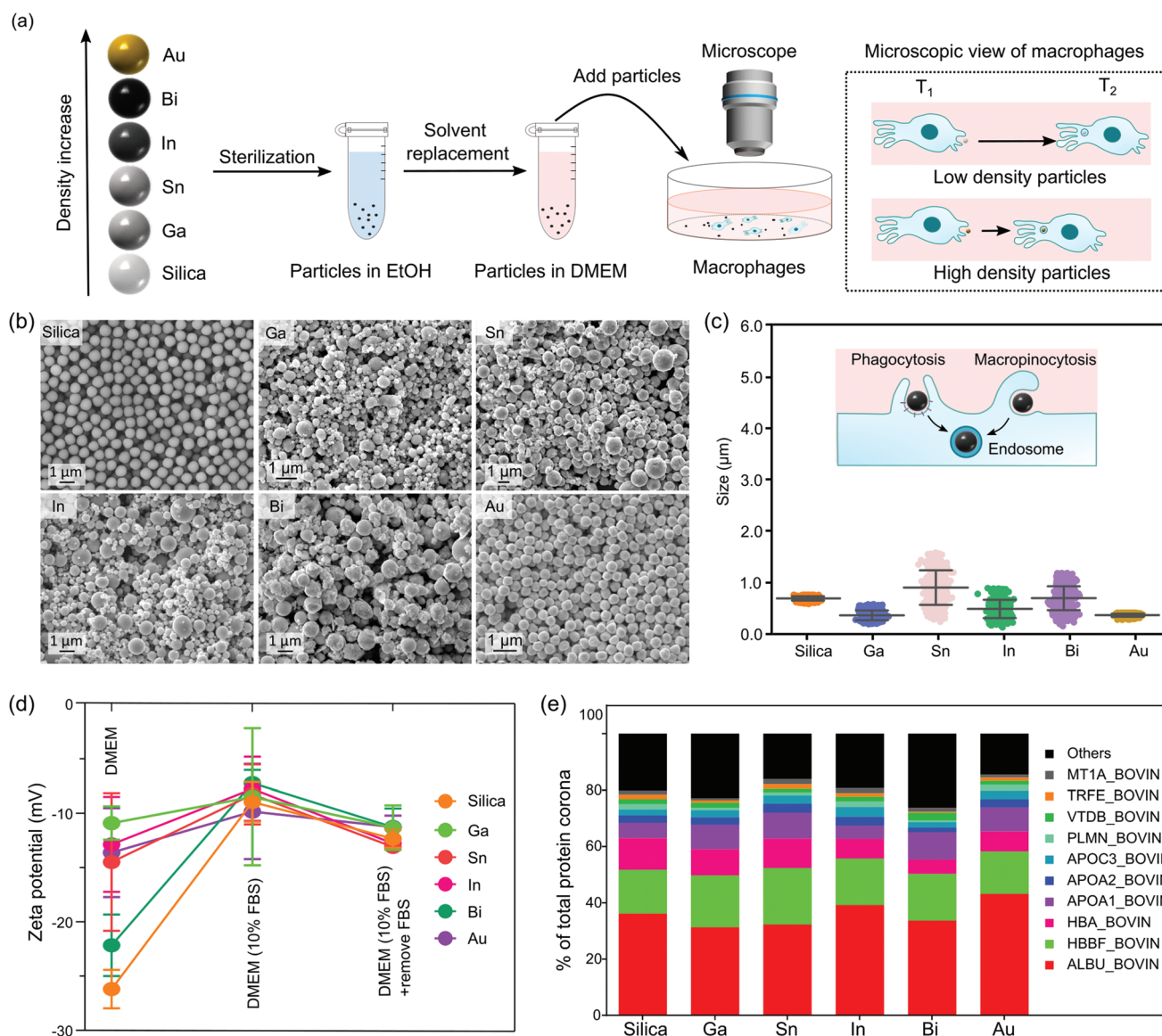
Figure 1. Preparation and morphological analyses of particles. a) Schematic illustration of treating RAW 264.7 macrophages with different particles (silica, Ga, Sn, In, Bi, and Au particles) of various densities. These particles are sterilized by EtOH and transferred into DMEM before adding into macrophages. The interactions between the cells and these particles are observed by optical microscopy. b,c) Representative SEM images (b) and size distributions (c) of silica, Ga, Sn, In, Bi, and Au particles. Experiments were performed at $n = 100$ and data are expressed as mean ± standard deviation. The suggested endocytosis of particles provided in the inserted schematic. d) Zeta potentials of particle suspensions were measured in these three settings: 1) DMEM: particles in DMEM alone; 2) DMEM (10% FBS): particles in DMEM supplemented with 10% FBS; 3) DMEM (10% FBS) + remove FBS: particles were incubated in DMEM supplemented with 10% FBS first, then wash away the free proteins from FBS and measured the zeta potentials of particle suspensions in DMEM alone. Experiments were performed at $n = 3$ and data are expressed as mean ± standard deviation. e) LC-MS/MS analysis of the "protein corona" formed on the surface of six types of particles. The concentration of particles is 8.31×10^{-6} cm^3 mL^{-1}. Experiments were performed at $n = 3$ and data are expressed as mean.

subunit alpha (HBA_BOVIN), apolipoprotein A-I (APOA1_BOVIN), apolipoprotein A-II (APOA2_BOVIN), apolipoprotein C-III (APOC3_BOVIN), plasminogen (PLMN_BOVIN),

vitamin D-binding protein (VTDB_BOVIN), serotransferrin (TRFE_BOVIN), and metallothionein-1A (MT1A_BOVIN)), which detected by LC-MS/MS, were comparable and consisted of ≈80% of the protein layer. The coating of "protein corona" that mainly composed of BSA existing on the particles' surfaces is similar for all the particles, therefore, what the cells "see" are corona-coated particles instead of their pristine surfaces. We believe the rapid, natural, and systematic formation of corona coatings provides similar interfacial properties for those different particles in the cell culture medium when FBS

Table 1. The densities of particles.

Particle density [g cm^{-3}]					
Silica	Ga	Sn	In	Bi	Au
1.98	6.10	7.28	7.31	9.75	19.32

ADVANCED
SCIENCE NEWS
www.advancedsciencenews.com

NANO · MICRO
small
www.small-journal.com

is added, which excludes the interference of the native surfaces of different particles.

2.2. Cellular Uptake of Particles with Different Densities by RAW 264.7 Macrophages

The detailed interactions between the particles and macrophages are illustrated in **Figure 2**a,c,e based on the cells' behaviors observed under microscopy during the incubation of cells with Ga (Figure 2b,d,f) and other particles (silica, In, Bi, Ag, and Au, Figures S4–S6, Supporting Information). It is interesting to observe that these particles, in individual or aggregated forms, interact with cells in different ways. Specifically, the individual particles can either float in the medium or temporarily adhere to the substrate (Figure 2a,b and

Figure S4, Supporting Information) through the adhesive spots (i.e., petri dish bottom) produced by the cell filopodia.[34] Thereafter, these individual particles were seen to be quickly engulfed by the cells as soon as the cell filopodia closely approached them (Figure 2c,d and Figure S5, Supporting Information). We assume the sticky spots released from the macrophages can increase the cellular uptake of particles because more particles can stay less mobile, on the substrate which increases their exposure time to the cells. On the other side, the aggregated particles (Figure 2e,f and Figure S6, Supporting Information), with larger total dimensions (more than 5 µm), can easily sink onto the substrate and cannot be engulfed directly by the cells. Instead, when crushed by the cells, they are first de-clustered into individual particles and then accumulated by the sticky filopodia, followed by engulfing into the cells. In these observations, we could not see any significant differences between
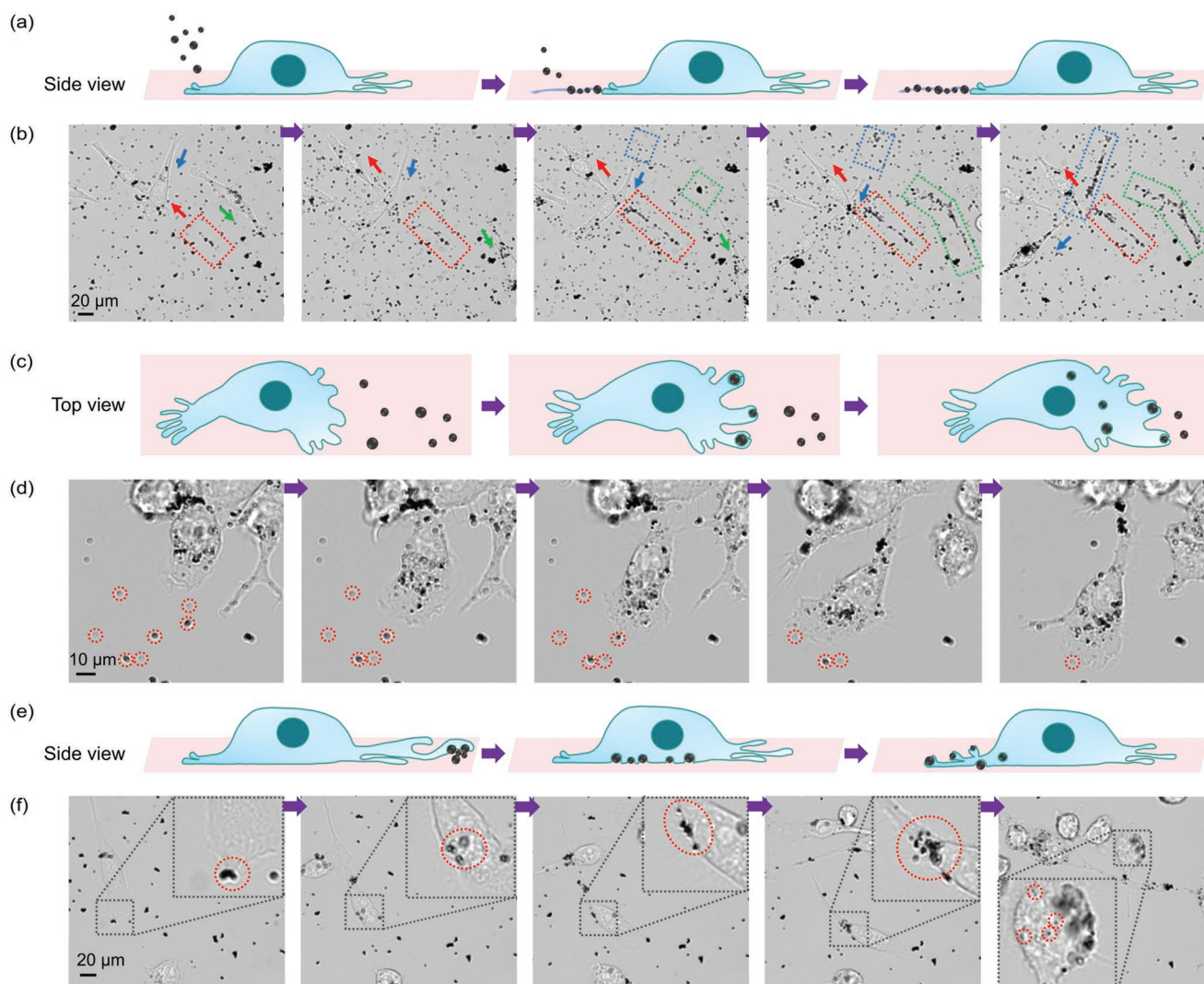
Figure 2. Interactions between particles and RAW 264.7 macrophages. Schematic illustration (a,c,e) and the optical view of Ga particles as an example (b,d,f). a,b) The floating individual particles stick to the adhesive spots produced by the cell filopodia and stay on the substrate. The arrows in (b) point out the moving directions of the cells and the dotted squares show the particles which stick to the adhesive spots. c,d) The process of individual particles being engulfed by macrophages. The Ga particles before being engulfed are circled by red dotted lines in (d). e,f) The interaction between cells and aggregated particles. The aggregated Ga particles are circled by the red dotted line in the optical images shown in (f).

ADVANCED
SCIENCE NEWS
www.advancedsciencenews.com

NANO · MICRO
small
www.small-journal.com

the particles of different densities regarding the generation of visible particle trails onto the adhesive spots and their cellular uptake processes.

2.3. The Influence of Particles on the Cell Viability of RAW 264.7 Macrophages

To assess the effect of different particles on macrophages, the cell viability was first measured when the cells were incubated with different concentrations of silica, Ga, Sn, In, Bi, and Au particles. As seen in **Figure 3**, none of the particles shows cytotoxicity for the provided concentrations within 12 h. As for the 48 h results, the safe concentration thresholds of silica, Ga, In, and Bi particles are 197.7, 244.2, 15.1, and 81 µg mL^{-1}, respectively, while the cell cytotoxicity for Sn and Au particles are not seen for up to 242 and 641.5 µg mL^{-1}. The cytotoxicity of silica and Ga on RAW 264.7 macrophages is consistent with the concentrations reported in the literature[35,36] and our previous work.[37] The In and Bi particles are less biocompatible, while Sn and Au particles show the best biocompatibility among those particles. The safe concentration thresholds from the cytotoxicity measurements for each particle were thereafter used as a guideline for choosing the experimental concentrations of those particles in the following experiments.

2.4. The Influence of Particles with Different Densities on the Motility of RAW 264.7 Macrophages

To assess the effects of particle densities on the motility of macrophages, we designed the experiments by exposing cells to each particle and used the time-lapse video recordings to track the cell movements. The concentrations of the particle suspension (V_p/V_m: the volume ratio of particles (cm^3) to the cell culture medium (mL)) shown in Table S1, Supporting Information, were chosen based on the safe concentration threshold of each particle type confirmed in Figure 3.

For comparing the effects of different types of particles on the macrophage mobility, we recorded the interactions between particles and the macrophages for at least 24 h but only used the recordings during the first 6 h after adding particles to decrease the cell culture environment alterations triggered by the secretion and deposition of the extracellular matrix components.[38] Then ten representative cells of each group were chosen to compare the cell behaviors (cell migration velocities and trajectories) in response to the particles' treatments. The cell migration velocities were measured every 10 min due to the large sample volume and long-time data processing. The instant cells migration velocity (v) at each sampling point was measured according to the illustration provided in Figure S7, Supporting Information, using the following equation:
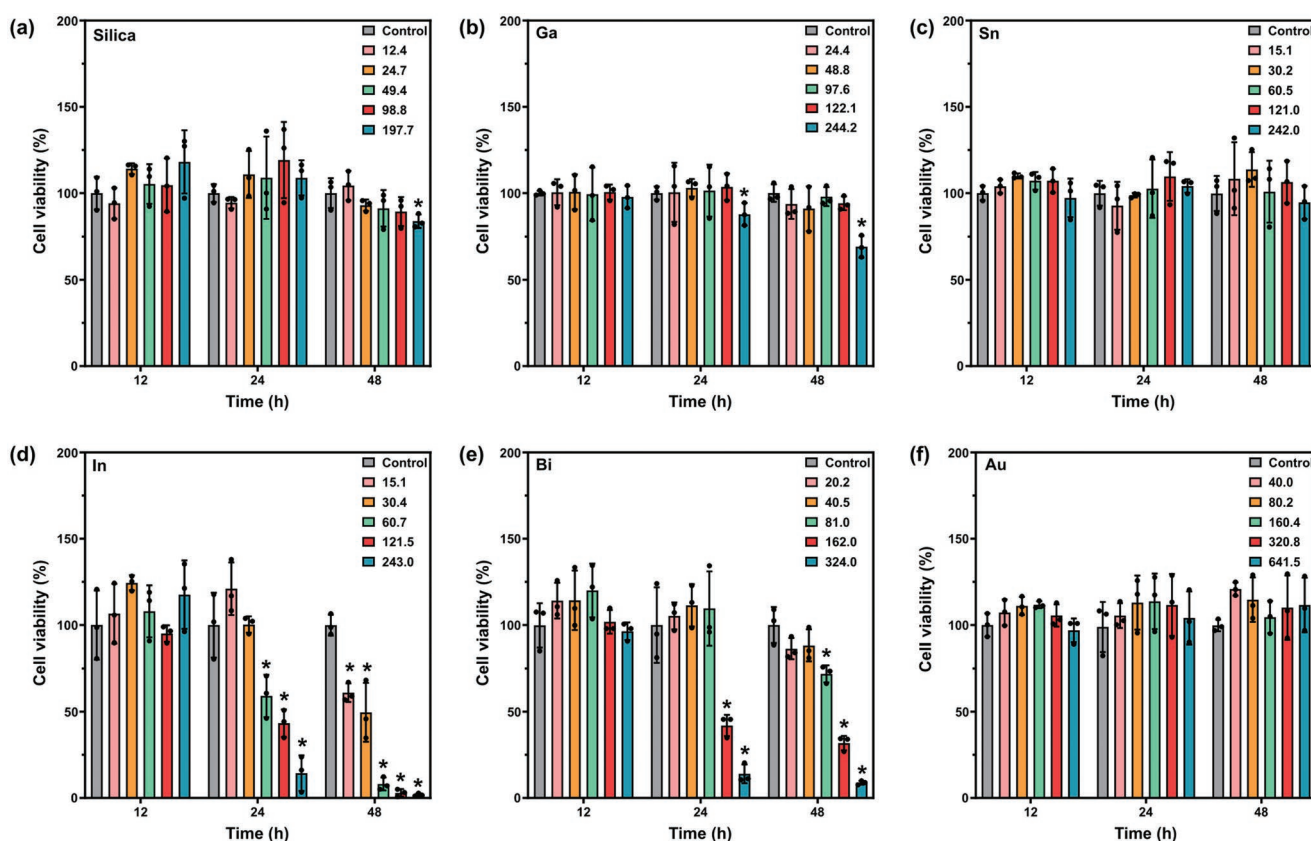
Figure 3. The cell viability of RAW 264.7 macrophages after being treated with different concentrations of each particle for 12, 24, and 48 h. a) Silica, b) Ga, c) Sn, d) In, e) Bi, and f) Au particles. The concentration unit for the particle suspensions is µg mL^{-1}. $p < 0.05$ is considered statistically significant and marks with *. Experiments were performed at $n = 3$ and data are expressed as mean ± standard deviation.

$$v = \frac{\Delta L}{\Delta t} = \frac{\sqrt{(x_2 - x_1)^2 + (y_2 - y_1)^2}}{t_2 - t_1} \quad (1)$$

In this case, x and y represent the coordinates of the cells and they were utilized to measure the cell migration distance (ΔL) between two locations. The time interval (Δt) between every two sampling points was 10 min.

As shown in **Figure 4**a–g and Figures S8 and S9, Supporting Information, the instant cell migration velocity for silica, Ga, and Sn at each sampling point within 6 h have fluctuating natures, while the velocities have fewer deviations when the cells were treated with In, Bi, and Au particles. It is interesting to see the total cell migration trajectories are shorter when the instant cell migration velocities are more stable. The higher concentration of those particles (Figure 4) shows more significant effects on cell motility than that with lower concentrations (Figures S8 and S9, Supporting Information), which indicates that the cell movements are also affected by the volume of particles that were engulfed inside.

To compare the effects of particle density and particle volume on cell mobility, the average cell migration velocity ($\overline{v}$) of macrophages within $t = 6$ h (36 sampling points in total) were calculated by adding the cell migration distance at each sampling point (ΔL_i) according to the following equation:

$$\overline{v} = \frac{\sum_{i=1}^{i=36} \Delta L_i}{t} \quad (2)$$

Comparing the $\overline{v}$ of macrophages treated with six types of particles (Figure 4h and Figures S10 and S11, Supporting Information), we can see that the $\overline{v}$ decreases with the increase of particle density (silica (1.98 g cm^{-3}) < Ga (6.10 g cm^{-3}) < Sn (7.28 g cm^{-3}) < In (7.31 g cm^{-3}) < Bi (9.75 g cm^{-3}) < Au (19.32 g cm^{-3})), the relationship between $\overline{v}$ and particle density can be fitted according to a second-order polynomial model as shown in Figure 4i. A decreasing trend for the average velocities of macrophages with increasing densities of particles can be seen. We observed that for Au and Bi particles, some of the macrophages almost stopped their migration after
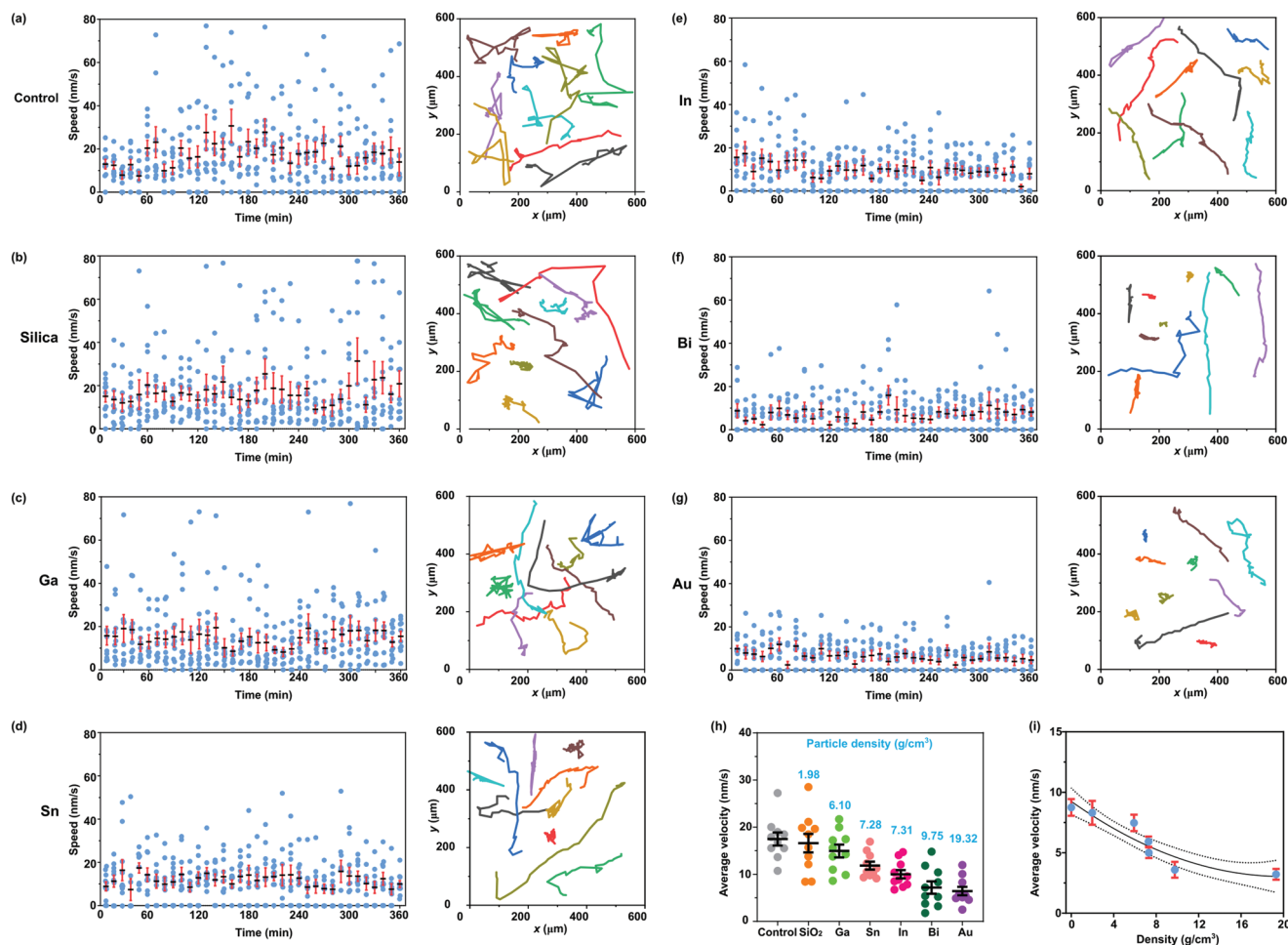
Figure 4. The average migration velocities of RAW 264.7 macrophages every 10 min within 6 h and the cell moving trajectories. The cells are recorded without particle treatment as a) control or incubated with b) silica, c) Ga, d) Sn, e) In, f) Bi, or g) Au particles, respectively. h) The average cell displacement velocities within 6 h when the RAW 264.7 macrophages were treated with six different types of particles. i) The relationship between $\overline{v}$ and particle densities can be fitted by a second-order polynomial. The concentrations for all the particles are equal to 8.31×10^{-6} cm^3 mL^{-1}. Experiments were performed at $n = 10$ and data are expressed as mean ± standard error of the mean.

6 h. These particles with very high densities, make the cells so immobile that some of them cannot migrate anymore.

We then focused on exploring the influence of particles' concentrations on the migration of the cells, the results presented in **Figure 5**a show that increasing the concentrations of particles can also contribute to a slight decrease in the migration velocities of cells. However, the impact is much smaller than that of the particles' densities. The higher particle concentrations (Figure 5b) are suggested to result in much more even cellular uptake of particles into the macrophages, while the uptake of particles is seen to be more stochastic in the groups of particles with lower concentrations (Figure S12, Supporting Information). The hypothesized cellular endocytosis of particles with different concentrations is illustrated in the schematic presented in Figure S13, Supporting Information.

To confirm the volume of the six types of particles that engulfed in the RAW 264.7 macrophages, the inductively coupled plasma-optical emission spectrometry (ICP-OES) was employed to quantitatively measure the total amount of engulfed particles and the detailed method is illustrated in the schematic of Figure 5c. The results presented in Figure 5d show that there is no significant difference in the cellular uptake between each particle type as all of the particles were endocytosed at a percentage of ≈45% (the median values between 40% to 50%) for the same original concentration of 8.31×10^{-6} cm^3 mL^{-1}, which indicates that comparable volumes of each type of particles were internalized by the macrophages.

To confirm whether the size difference of particles can compromise the effect of particles' densities on the cell mobility, Ga particles of various sizes (1096.8 ± 221.3, 675.7 ± 197.6, 471.1 ± 125.3, and 338 ± 95 nm), presented in **Figure 6**a–d, were utilized as an example to assess the impact of size difference on the $\bar{v}$ of the RAW 264.7 macrophages. The example was presented for Ga particles because they could be relatively easily made at different dimensions using a sonication/centrifuge process. As shown in Figure 6e–h, there is no discernable difference between the $\bar{v}$ of RAW 264.7 macrophages when treated with Ga particles of four different sizes within 6 h. These results indicate that the size of particles within the tested range from 338 ± 95 to 1096.8 ± 221.3 nm does not contribute to a considerable difference in the mobility of macrophages.

Altogether, after eliminating the possible interfering factors from the surfaces of particles and particles' sizes, we conclude that in the scenario of exposing macrophages to nano/micro-sized heavy particles, a cell's motility is affected by the density of engulfed particles. This work is a reminder that when nano/microparticles are designed to be used for drug delivery, disease therapy, and other biomedical applications, their densities should be taken into consideration as they may affect the migratory behaviors of immune cells. Mechanistic studies for understanding the roles of particles' densities on the cells' movements are important. In future studies, further in-depth investigations should be implemented for a more fundamental comprehension of the phenomenon. Furthermore, while this study only focuses on investigating the influence of the inorganic particles' densities on the mobility of macrophages, we believe it would also be very interesting to similarly study the impacts of organic particles, such as the polymeric and lipid-based particles, on the migratory behaviors of the cells.

3. Conclusions

In this work, we delivered several types of inorganic nano/microparticles with different densities into RAW 264.7 macrophages and observed their interactions with these cells. The cellular uptake of the particles by macrophages was recorded under light microscopy. The particles of different densities did not show significant differences in the phagocytosis of macrophages and they all could be successfully engulfed by the cells. The interference from different surface characteristics of those particles was seen to be reduced by the BSA "protein corona" formation on the surfaces of the particles assuring that the impact was only due to the density. The safe threshold concentrations were assessed by the cytotoxicity tests and they were consequently used for choosing the particle concentrations in the later experiments. After comparing the effects of particles with different densities on cell motility, we found that the cell migration velocity and trajectories were dominantly affected by the density of particles. The engulfment of particles of higher density resulted in lower cell migration velocities and generally shorter migration tracks as follows: Au (19.32 g cm^{-3}) < Bi (9.75 g cm^{-3}) < In (7.31 g cm^{-3}) < Sn (7.28 g cm^{-3}) < Ga (6.10 g cm^{-3}) < silica (1.98 g cm^{-3}). It reveals the rule that engulfed particles with a higher density can reduce the migration ability of macrophages. This work provides a microscopic view for understanding the mechanistic interactions between particles of different densities and macrophages, and adds a crucial reminder to the field of nanomedicine that the particles' densities should be carefully considered for their utilization in biological applications.

4. Experimental Section

Materials: Metallic Ga (purity >99.99%), In (purity >99.99%), Bi (purity >99.99%), and Sn (purity >99.99%) were purchased from Rotometals, USA. The Au particles, DMEM (low glucose, low glucose, Cata. No. 11 885 084), FBS (Cata. No. 12003C), and L-glutamine solution (200 mM, Cata. No. G7513) were purchased from Sigma-Aldrich, Australia. Silica particles, Simplyblue (Cata. No.: LC6060), NuPAGE Bis-Tris gels (Cata. No.:NP0315BOX), protein loading buffer (Cata. No.: NP0007), and RIPA cell lysis buffer (Cata. No.: 89 900) were bought from Thermo Fisher Scientific Australia Pty Ltd. Blue pre-stained protein marker (Cata. No.: 59 329) was purchased from Cell Signaling Technology (Beverly, MA, USA). Cell Counting Kit 8 (CCK8, Cata. No. ab228554) was bought from Abcam, UK. Silicon oil (silicone 200 fluid, boiling point >300 °C), glycerol, and EtOH (100%, unsaturated) were obtained from Chem-supply (Australia). Chloroform (99.8%) was purchased from RCI Labscan. The RAW 264.7 macrophages were bought from American Type Culture Collection (ATCC), USA.

Preparation of Particles using a Liquid Metal-Based Process: Ga, In, Bi, and Sn particles were all synthesized by ultrasonication using a probe sonicator (Sonics VCX 750, Sonics & Materials, Inc.).[37,39,40] Briefly, a bulk metal was heated to melt and added with a medium (10 mL) in a glass vial with/without a bath that was placed on a hot plate. A probe (diameter: 6 mm) was immersed into the metal-medium mixture, which was then sonicated with a burst mode (on/off) for a certain period. Temperatures of the used baths or glass vial bottoms were controlled by the hot plate during the sonication process. Specific sonication parameters for each metal are listed in Table S2, Supporting Information. After sonication, Ga and In particles were washed with EtOH thoroughly, whereas Bi and Sn particles were first washed with chloroform and then EtOH. All the particles were then stored in EtOH and were washed with
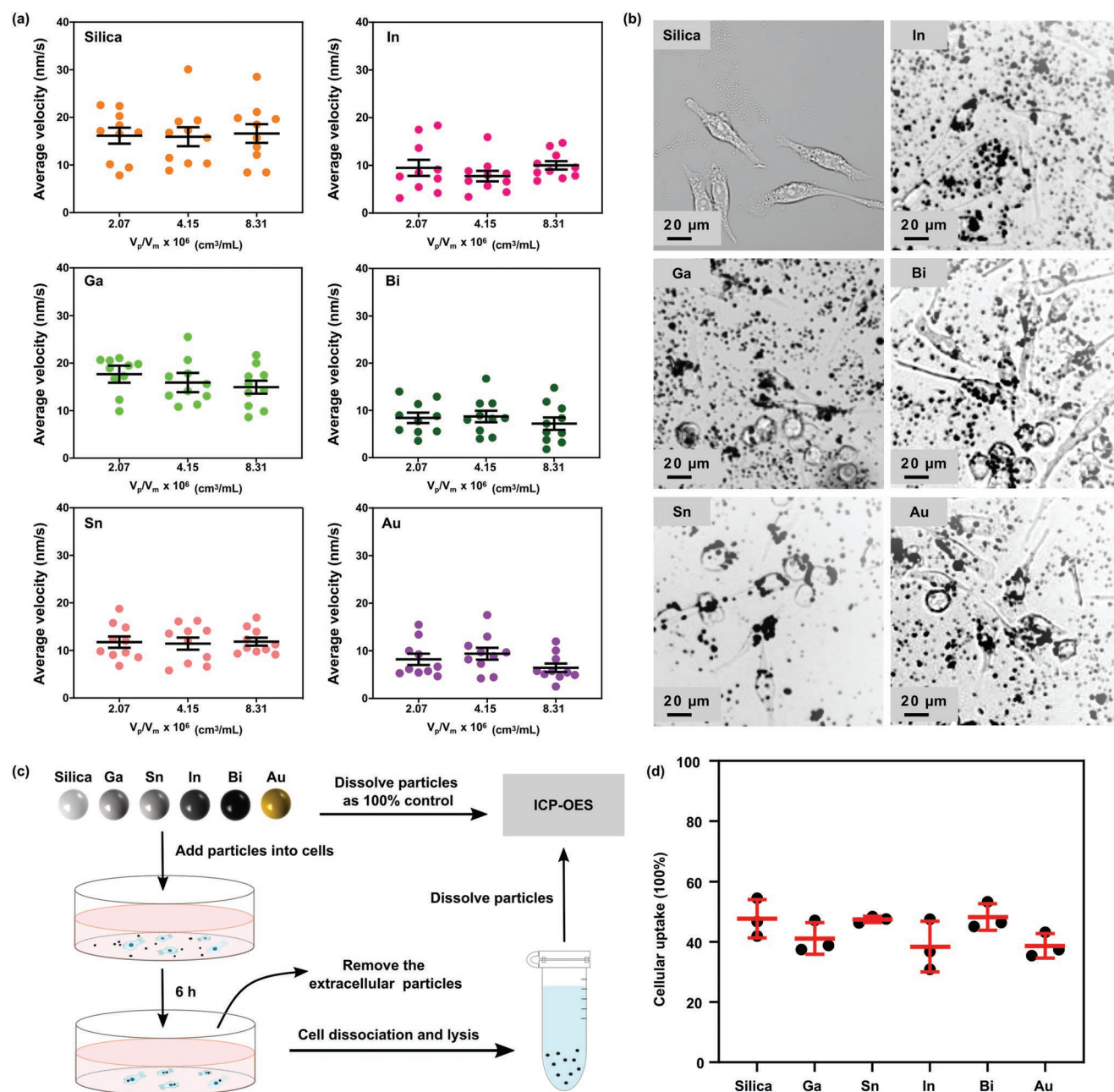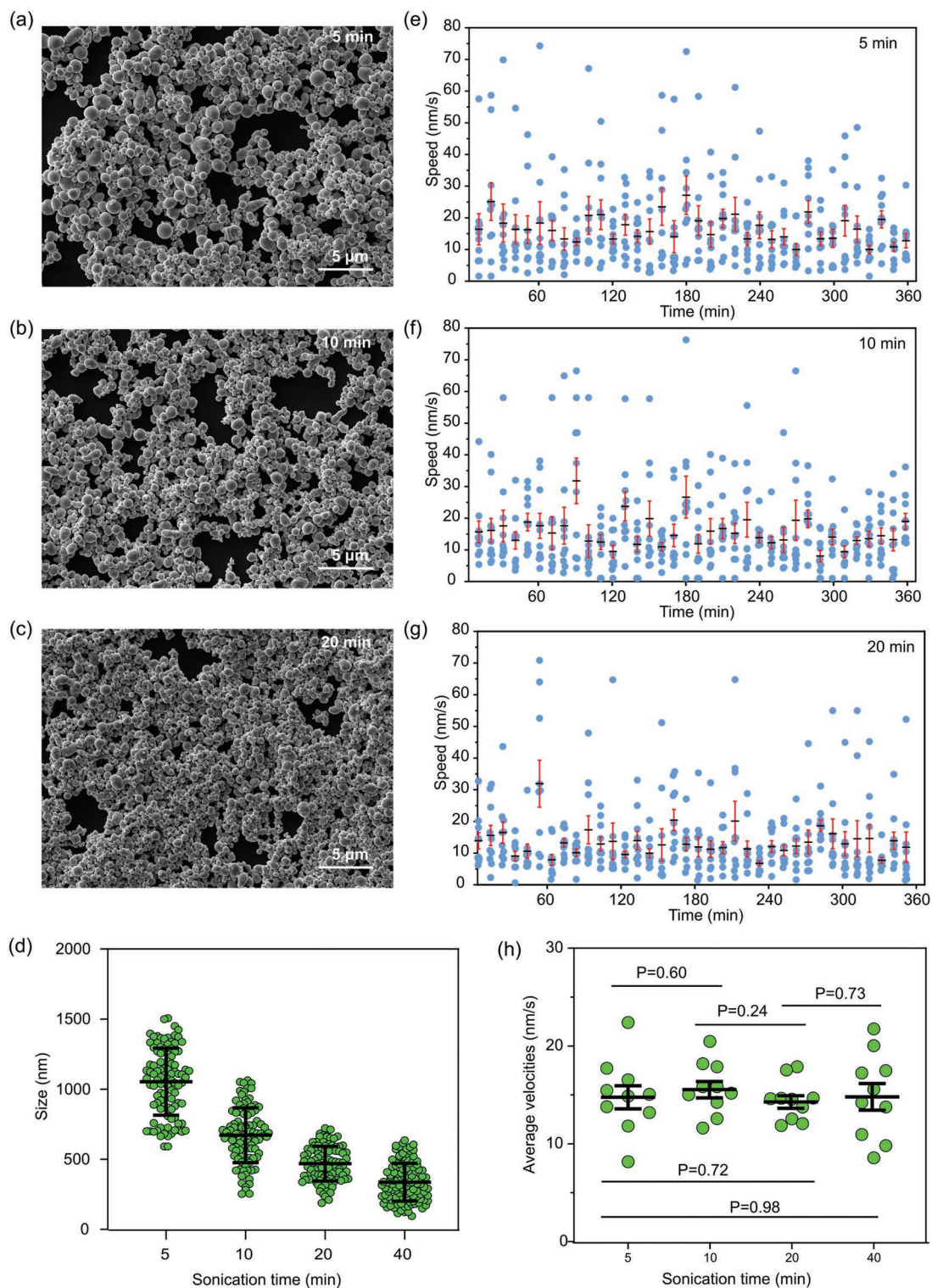
Figure 5. Comparing the impact of particles' concentrations on the migration of RAW 264.7 macrophages and the assessment of the cellular uptake of particles in the macrophages. a) The average cell velocities within 6 h when the cells were treated with silica, Ga, Sn, In, Bi, and Au particles at the concentrations of: 2.07×10^{-6}, 4.15×10^{-6}, and 8.31×10^{-6} cm³ mL⁻¹, respectively. Experiments were performed at $n = 10$ and data are expressed as mean ± standard error of the mean. b) The optical microscope view of RAW 264.7 macrophages treated with silica, Ga, Sn, In, Bi, and Au at the concentrations of 8.31×10^{-6} cm³ mL⁻¹. c) Schematic representation of the process for preparing samples for ICP-OES analysis. The particles were dissolved by strong acids or bases as described in the Experimental Section. d) The percentage of the cellular uptake of the six types of particles in the RAW 264.7 macrophages at the concentrations of 8.31×10^{-6} cm³ mL⁻¹. Experiments were performed at $n = 3$ and data are expressed as mean ± standard deviation.

sodium phosphate buffer solution three times prior to use. For preparing Ga particles with different dimensions, according to the methods reported previously, the Ga bulks were sonicated for 5, 10, and 20 min, respectively.

Morphology Characterization of Particles: Morphologies of the metal particles were characterized by SEM (JEOL InTouchScope, JSM-IT 500 HR). Size distributions of metal particles were determined using the ImageJ software (National Institutes of Health, United States).

Assessment of the Zeta Potentials and Hydrodynamic Particle Sizes of the Particles: The six types of particles with the same concentration (8.31×10^{-6} cm³ mL⁻¹) were incubated with 1 mL DMEM (supplemented with 10% FBS and 1% L-glutamine solution) in a humidified incubator (37 °C, 5% CO₂) for 30 min. Then the particles were washed with PBS thrice and suspended in DMEM for the measurements of particle size distributions and zeta potentials by using a Zetasizer Ultra (Malvern Instruments Ltd., UK).

**ADVANCED
SCIENCE NEWS**

www.advancedsciencenews.com

NANO · MICRO

small

www.small-journal.com

Figure 6. Comparing the average migration speed of RAW264.7 macrophages treated with Ga particles of different sizes. a–c) Representative SEM images of Ga particles synthesized by sonicating Ga bulks for 5, 10, and 20 min, respectively. d) Size distributions of Ga particles sonicated for 5, 10, 20, and 40 min are extracted from the SEM images presented in (a–c) and Figure 1b, respectively Experiments were performed at $n = 100$ and reported as mean ± standard deviation. e–g) The average migration velocities of RAW 264.7 macrophages every 10 min within 6 h after their exposure to Ga particles which were synthesized by sonicating Ga bulks for 5, 10, and 20 min, respectively. Experiments were performed at $n = 10$ and reported as mean ± standard error of the mean. h) The average cell velocities within 6 h when the RAW 264.7 macrophages were treated with Ga particles synthesized by sonicating Ga bulks for 5, 10, 20, and 40 min, respectively. Experiments were performed at $n = 10$ and reported as mean ± standard error of the mean. The concentration of Ga particles used in (e)–(h) is 8.31×10^{-6} cm^3 mL^{-1}. p-Value of <0.05 is considered as a significant difference.

Cell Culture for RAW 264.7 Macrophages: The RAW 264.7 macrophages were cultured in DMEM, which was supplemented with 10% FBS and 1% L-glutamine solution in a humidified incubator (37 °C, 5% CO_2). During the incubation or subculture for experiments, the medium was changed every 2 days when the cells reached 80% of confluence.

Cell Viability/Metabolic Activity: To assess the effects of particles on the cell viability/metabolic activity of RAW 264.7 macrophages, the cells (10^4/well) were first seeded in 96-well plates and cultured for 24 h, then were treated with different concentrations of particles (Ga, In, Bi, Sn, silica, and Au) for another 12, 24, and 48 h. Afterward, the medium was replaced with a fresh medium that contained 10% of CCK8 and was subsequently incubated for another 90 min. To exclude the background absorbance from the cells and particles, the supernatant of the medium was gently transferred to a new 96-well plate, where the absorbance at 460 nm of each well was read and recorded using a microplate reader (Clariostar Plus, BMG Labtech). The absorbances of cell-free medium with different particles were recorded as references.

High-Resolution Live Cell Imaging System: To record the cell migration, the particles are added to the glass-bottom 12-well plates, where the RAW 264.7 macrophages (10^5/well) had been seeded for 24 h. The 12-well plates were then placed in an imaging chamber (37 °C, 5% CO_2) of a high-resolution microscopy system (Cell Discoverer 7, Zeiss), where the images were captured every 10 min. The position of the nucleus center of individual cells (only isolated and spindle-shaped cells were chosen) in the first 6 h time-lapse images was marked by Photoshop (Adobe Inc.) and the cell trajectories were analyzed using a Photoshop script. The average migration velocities, migration areas, as well as the deviations of cells migrated along the x and y axis (in the reference frame of the recorded images) were analyzed based on the cell migration trajectories.

The Quantitative Measurement of Cellular Uptake of Particles: To assess the cellular uptake of particles in macrophages, six types of particles with the same concentrations (8.31×10^{-6} cm^3 mL^{-1}) were added into 25 cm^2 flasks, respectively, where the RAW 264.7 macrophages (5×10^5/well) had been seeded for 24 h. After the incubation for 6 h, the extracellular particles were washed away with PBS three times. Later on, the cells were dissociated by trypsin and then lysed by cell lysis buffer. The cell lysates were then added with different types of strong acids or bases to dissolve the particles. In detail, 4 M hot sodium hydroxide, 1 M nitric acid, and freshly prepared aqua regia were used to dissolve silica, Bi, and Au particles, respectively, while 1 M hydrochloride acid was used for Ga, Sn, and In particles. The concentrations of each element in the cell lysates were assessed using ICP-OES (PerkinElmer, USA) process. The same concentration of each particle (without the cell incubation) was dissolved directly by the acid or base and measured by ICP-OES as 100% control.

Protein Analysis Using Shotgun LC-MS/MS Proteomics: To determine the formation of the protein corona on the surfaces of particles, a proteomic study was utilized to identify the proteins by using LC-MS/MS analysis. The six types of particles were mixed with DMEM (supplemented with 10% FBS) at the concentration of 8.31×10^{-6} cm^3 mL^{-1} and incubated at 37 °C with shaking for 60 min. To obtain hard protein corona complexes, the samples were centrifuged for 5 min at 8000 g to obtain the pellet and re-suspended in PBS three times. Immediately after the last centrifugation step, the particle-protein corona pellets were collected and stored at −30 °C until analyzed.

The samples were re-suspended in 100 μL 50 mM ammonium bicarbonate (NH_4HCO_3) and the protein content of the sample was reduced by 5 mM dithiothreitol at 37 °C for 30 min. Afterward, the cysteine residues of the proteins were alkylated using 10 mM iodoacetate in a dark room with ambient temperature. The samples were then digested by trypsin overnight. Digested peptides were analyzed using a nanoLC instrument equipped with an Ultimate nanoRSLC ultra-performance liquid chromatography (UPLC) and autosampler system (Dionex, Amsterdam, Netherlands). Before the chromatographic separation, samples (2.5 μL) were desalted and preconcentrated onto a micro C_{18} pre-column (300 μm × 5 mm, Dionex) with H_2O:CH_3CN (98:2, 0.2% TFA) at 15 μL min^{-1} and the pre-column was washed for 4 min. Next, the injection port (Valco 10 port UPLC valve, Valco, Houston, TX) was switched to introduce the sample into a fritless nano column (75 μm × 15 cm) containing C18AQ media (1.9 μm, 120 Å, Dr. Maisch, Ammerbuch-Entringen, Germany). Linear gradient elution of H_2O:CH_3CN (98:2) to H_2O:CH_3CN (64:36) with the speed at 200 nL min^{-1} over 30 min was employed to separate peptides. Separated peptides were detected by applying a voltage of 2000 V to a low volume Titanium union (Valco, Houston, TX) and the tip positioned ≈0.5 cm from the heated capillary (temperature: 275 °C) of an Orbitrap Fusion Lumos (Thermo Electron, Bremen, Germany) mass spectrometer. Mass spectra were collected in positive ion mode electrospray ionization operated in data-dependent acquisition mode . Results were acquired within m/z 350–1750 with mass resolutions as high as 120000, accumulation target value of 400000 ions, and lock mass was enabled at m/z 445.12003. A top-speed approach (cycle time: 2s) was utilized to perform data-dependent tandem MS analysis. The HCD (NCE = 30) activation mode was used to fragment the MS2 spectra, and the ion trap was selected as the mass analyzer. The intensity threshold for the peptide fragmentation was set at 25000. A dynamic exclusion of 20 s was applied (mass tolerance: 10 ppm).

Results were analyzed by Mascot Daemon/Mascot Distiller (Matrix Science, London, UK) and submitted to the database search program Mascot (version 2.5.1, Matrix Science). Search parameters were set as follows: precursor tolerance 4 ppm, product ion tolerances ± 0.4 Da; Oxidation and carboxyamidomethyl specified as variable modification, enzyme specificity was trypsin, two missed cleavages were considered, and the Uniprot database was used to search. Only protein hits with scores >50 were considered statistically significant, and each identified protein's relative abundances were calculated according to the respective exponentially modified protein abundance index (emPAI).[41]

Sample Preparation for the Transmission Electron Microscopy Images: The RAW 264.7 macrophages (10^5/well) were seeded onto a 12-well plate (round sterile glass coverslips were placed inside) for 24 h and treated with six types of each particle at the concentration of 8.31×10^{-6} cm^3 mL^{-1} for 4 h. After the treatment, the samples were fixed by 2.5% glutaraldehyde, dehydrated by EtOH, and infiltrated with resin (Procure, 812) according to a standard protocol. The samples were then cut into ultrathin sections, to the thickness of ≈70 nm, using a diamond knife (Diatome). They then transferred onto holey carbon-coated copper TEM grids for imaging to be conducted using a TEM (JEOL TEM-1400, Japan) operating at 100 kV.

Statistical Analysis: Each experiment was repeated three times with replicates in each assay. Data were presented as mean ± standard deviation or standard error of the mean. The one-way ANOVA in Prism 8.0.2 (GraphPad Software Inc.) was utilized to assess the statistically significant differences between the control group and the experimental groups. $p < 0.05$ was considered as statistically significant and marked with *.

Supporting Information

Supporting Information is available from the Wiley Online Library or from the author.

Acknowledgements

Conflict of Interest

The authors declare no conflict of interest.

Author Contributions

C.Z. did the preliminary experimental observations. C.Z. and K.K.-Z. conceived the ideas and designed the experiments. C.Z. conducted the main experiments and characterizations and analyzed the data. J.T., W.X., and F.-M.A. helped with drawing the schematic and revising the manuscript. Z.C. helped with the measurement of zeta potential and DLS particle size distribution. J.M.B. contributed to the TEM sample preparation, imaging, and data analysis. M.T. helped with analyzing the LC-MS/MS results. F.D., Y.L., R.A., M.B., M.M., and D.E. helped with the data analysis. The first manuscript was drafted by C.Z. and received input from all the other authors.

Data Availability Statement

The data that support the findings of this study are available from the corresponding author upon reasonable request.

Keywords

inorganic particles, macrophages, mechanistic observation, migration, particle density

[1] M. Liong, J. Lu, M. Kovochich, T. Xia, S. G. Ruehm, A. E. Nel, F. Tamanoi, J. I. Zink, *ACS Nano* **2008**, *2*, 889.

[2] D. Wang, W. Xie, Q. Gao, H. Yan, J. Zhang, J. Lu, B. Liaw, Z. Guo, F. Gao, L. Yin, G. Zhang, L. Zhao, *Small* **2019**, *15*, 1900511.

[3] J. L. Vivero-Escoto, I. I. Slowing, B. G. Trewyn, V. S.-Y. Lin, *Small* **2010**, *6*, 1952.

[4] Q. Yun, A. Kimura, M. Taguchi, E. Miyako, *Appl. Mater. Today* **2022**, *26*, 101302.

[5] Y. Yu, E. Miyako, *iScience* **2018**, *3*, 134.

[6] Y. Ren, M. Duan, R. Guo, J. Liu, *Sensors* **2021**, *21*, 6329.

[7] S. Zhang, W. Ni, X. Kou, M. H. Yeung, L. Sun, J. Wang, C. Yan, *Adv. Funct. Mater.* **2007**, *17*, 3258.

[8] Y. Hui, X. Yi, F. Hou, D. Wibowo, F. Zhang, D. Zhao, H. Gao, C.-X. Zhao, *ACS Nano* **2019**, *13*, 7410.

[9] Y. Li, X. Zhang, D. Cao, *Nanoscale* **2015**, *7*, 2758.

[10] N. Hao, L. Li, F. Tang, *Int. Mater. Rev.* **2017**, *62*, 57.

[11] Q. Wang, Y. Yu, J. Liu, *Adv. Eng. Mater.* **2018**, *20*, 1700781.

[12] S. D. Perrault, C. Walkey, T. Jennings, H. C. Fischer, W. C. W. Chan, *Nano Lett.* **2009**, *9*, 1909.

[13] K. C. L. Black, Y. Wang, H. P. Luehmann, X. Cai, W. Xing, B. Pang, Y. Zhao, C. S. Cutler, L. V. Wang, Y. Liu, Y. Xia, *ACS Nano* **2014**, *8*, 4385.

[14] R. Mo, T. Jiang, Z. Gu, *Angew. Chem., Int. Ed.* **2014**, *53*, 5815.

[15] Y. Lu, Q. Hu, Y. Lin, D. B. Pacardo, C. Wang, W. Sun, F. S. Ligler, M. D. Dickey, Z. Gu, *Nat. Commun.* **2015**, *6*, 10066.

[16] P. Decuzzi, S. Lee, B. Bhushan, M. Ferrari, *Ann. Biomed. Eng.* **2005**, *33*, 179.

[17] R. Toy, E. Hayden, C. Shoup, H. Baskaran, E. Karathanasis, *Nanotechnology* **2011**, *22*, 115101.

[18] A. J. Thompson, O. Eniola-Adefeso, *Acta Biomater.* **2015**, *21*, 99.

[19] C. Y. Tay, M. I. Setyawati, D. T. Leong, *ACS Nano* **2017**, *11*, 2764.

[20] E. Blanco, H. Shen, M. Ferrari, *Nat. Biotechnol.* **2015**, *33*, 941.

[21] D. Rosenblum, N. Joshi, W. Tao, J. M. Karp, D. Peer, *Nat. Commun.* **2018**, *9*, 1410.

[22] D. A. Fedosov, J. Fornleitner, G. Gompper, *Phys. Rev. Lett.* **2012**, *108*, 028104.

[23] D. C. Dale, L. Boxer, W. C. Liles, *Blood* **2008**, *112*, 935.

[24] S. Gordon, A. Plüddemann, *BMC Biol.* **2017**, *15*, 53.

[25] S. Epelman, K. J. Lavine, G. J. Randolph, *Immunity* **2014**, *41*, 21.

[26] H. H. Gustafson, D. Holt-Casper, D. W. Grainger, H. Ghandehari, *Nano Today* **2015**, *10*, 487.

[27] J. Liu, Z. Liu, Y. Pang, H. Zhou, *J. Nanobiotechnol.* **2022**, *20*, 127.

[28] W.-J. Gao, J.-X. Liu, Y. Xie, P. Luo, Z.-Q. Liu, L. Liu, H. Zhou, *Pharmacol. Res.* **2021**, *167*, 105513.

[29] P. Krzyszczyk, R. Schloss, A. Palmer, F. Berthiaume, *Front. Physiol.* **2018**, *9*, 419.

[30] S. A. MacParland, K. M. Tsoi, B. Ouyang, X.-Z. Ma, J. Manuel, A. Fawaz, M. A. Ostrowski, B. A. Alman, A. Zilman, W. C. W. Chan, I. D. McGilvray, *ACS Nano* **2017**, *11*, 2428.

[31] M. Nahrendorf, H. Zhang, S. Hembrador, P. Panizzi, D. E. Sosnovik, E. Aikawa, P. Libby, F. K. Swirski, R. Weissleder, *Circulation* **2008**, *117*, 379.

[32] S. Behzadi, V. Serpooshan, W. Tao, M. A. Hamaly, M. Y. Alkawareek, E. C. Dreaden, D. Brown, A. M. Alkilany, O. C. Farokhzad, M. Mahmoudi, *Chem. Soc. Rev.* **2017**, *46*, 4218.

[33] J. P. Lim, P. A. Gleeson, *Immunol. Cell Biol.* **2011**, *89*, 836.

[34] J. Albuschies, V. Vogel, *Sci. Rep.* **2013**, *3*, 1658.

[35] L. Chen, J. Liu, Y. Zhang, G. Zhang, Y. Kang, A. Chen, X. Feng, L. Shao, *Nanomedicine* **2018**, *13*, 1939.

[36] M. Kersting, M. Olejnik, N. Rosenkranz, K. Loza, M. Breisch, A. Rostek, G. Westphal, J. Bünger, N. Ziegler, A. Ludwig, M. Köller, C. Sengstock, M. Epple, *Sci. Rep.* **2020**, *10*, 21591.

[37] C. Zhang, B. Yang, J. M. Biazik, R. F. Webster, W. Xie, J. Tang, F.-M. Allioux, R. Abbasi, M. Mousavi, E. M. Goldys, K. A. Kilian, R. Chandrawati, D. Esrafilzadeh, K. Kalantar-Zadeh, *ACS Nano* **2022**, *16*, 8891.

[38] J. Winkler, A. Abisoye-Ogunniyan, K. J. Metcalf, Z. Werb, *Nat. Commun.* **2020**, *11*, 5120.

[39] Y. Chi, J. Han, J. Zheng, J. Yang, Z. Cao, M. B. Ghasemian, M. A. Rahim, K. Kalantar-Zadeh, P. Kumar, J. Tang, *ACS Appl. Mater. Interfaces* **2022**, *14*, 30112.

[40] S.-Y. Tang, D. R. G. Mitchell, Q. Zhao, D. Yuan, G. Yun, Y. Zhang, R. Qiao, Y. Lin, M. D. Dickey, W. Li, *Matter* **2019**, *1*, 192.

[41] Y. Chen, J. Zhang, G. Xing, Y. Zhao, *J. Proteome Res.* **2009**, *8*, 3141.